Detailed Model for Transient Liquid Flow in Heat Pipe Wicks

J. H. Ambrose* and L. C. Chow†
University of Kentucky, Lexington, Kentucky 40506
and
J. E. Beam‡
Wright Research and Development Center, Wright-Patterson Air Force Base, Ohio 45433

Transient liquid flow in a low-temperature, homogeneous wick heat pipe is investigated experimentally and analytically for pulsed heat load conditions. The continuous distribution of the liquid in the wick is modeled, where previous models had assumed a uniformly saturated structure. A heat pipe with beryllium walls was used to obtain transient measurements of the saturation distribution in the wick structure using x-ray radiography. Analytical and experimental results are presented for the axial liquid distribution in the wick as a function of time. Transient liquid distributions for the model and experiment compare favorably. These results show that significant reductions in saturation may occur in the evaporator region for higher heat loads. These reductions affect the wick-flow properties and must be included in the liquid-flow analysis.

Nomenclature

A = area, m^2
$f(S)$ = moisture diffusivity, kg·m/s, Eq. (6)
J = source term, s^{-1}, Eq. (5)
K = full permeability, m^2
K_r = relative permeability
L = length, m
m = mass of liquid in pores, kg
$\dot{m}$ = mass flow rate, kg/s
P = pressure, Pa
P_c = capillary pressure, Pa
Q = heat transfer rate, w
S = saturation (ratio of liquid volume to void volume)
S_i = irreducible saturation
T = temperature, °C
t = time, s
x = position coordinate, m
ε = wick porosity
λ = latent heat of vaporization, J/kg
μ = dynamic viscosity of liquid, kg/m·s
ρ = density of liquid, kg/m^3
σ = surface tension, N/m
ϕ = reduced saturation ($\phi = S - S_i/1 - S_i$)

Subscripts
c = condenser section
e = evaporator section
tot = total
v = vapor
w = wick cross section

Introduction

THE present research was motivated by the need for detailed and accurate modeling of transient heat pipe performance. During pulsed heat loading, significant gradients in saturation usually occur, and local drying of the wick may also occur. These phenomena may drastically affect the overall heat transport of a device and the temperature distribution.

A detailed model of the liquid flow in the heat pipe wick is necessary to obtain more accurate predictions of transient behavior. The capillary pumping and permeability which control the local movement of liquid in the wick are both known to be functions of the amount of liquid present locally, or the saturation. Thus, in a realistic model, the saturation dependence of the liquid flow must be included. This hypothesis is supported by the extensive research efforts to model fluid flow in geological formations.

The actual heat and mass transfer processes occurring in the heat pipe wick during transient operation are much more complex than those of simplified heat pipe models. Because of the complex geometry of porous wicks, the capillary flow properties must be determined experimentally even for the fully saturated case. The saturation dependence of these properties must also be experimentally verified. If a detailed local model is to be useful for modeling heat pipe behavior, it must first be compared with the experiment. Thus, a detailed measurement of the liquid movement in the wick of an operating heat pipe is required.

Saturation measurements in heat pipes have been obtained in the past. However, these measurements are all limited to the case of steady-state operation. Moss and Kelly[1] imaged water in a thick, stainless-steel mesh wick, including the area in which evaporation took place. Merrigan et al.[2] imaged lithium working fluid in a heat pipe using neutron radiography. Shishido et al.[3] measured saturation distributions in a heat pipe with wicks of glass spheres and crushed brick powder using an electrical capacitance technique. Several researchers have utilized x-ray radiography to measure steady saturations in geologically significant materials.[4-6]

Theory

The transient liquid flow model is based on conservation of mass and momentum. The momentum balance is introduced in the form of Darcy's Law with saturation as the dependent variable. Mass flow rates of vapor into and out of the wick are assumed to be known from a decoupled energy balance.

Consider the control volume shown in Fig. 1, representing a small element of a wick structure. This control volume has

Presented as Paper 90-0062 at the AIAA 28th Aerospace Sciences Meeting, Reno, NV, Jan. 8–11; received Jan. 29, 1990; revision received Aug. 24, 1990; accepted for publication Sept. 30, 1990.

*Research Assistant; currently, Associate Research Scientist, m/s O/77-60, B/551, Lockheed Missiles and Space Co., 1111 Lockheed Way, Sunnyvale, CA 94084-3504. Member AIAA.
†Professor of Mechanical Engineering. Member AIAA.
‡Technical Area Manager. Member AIAA.

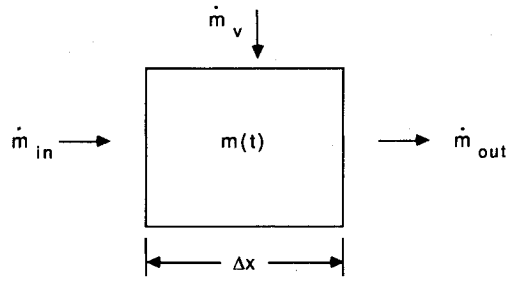

Fig. 1 Wick control volume.

a mass of liquid associated with it. The mass conservation equation is written for the control volume

$$\dot{m}_{in} - \dot{m}_{out} + \dot{m}_v = \frac{\partial m}{\partial t} \tag{1}$$

where $\dot{m}$ is liquid mass flow rate across the boundaries of the control volume, m is mass of liquid residing in the control volume, and $\dot{m}_v$ is the mass flow rate of vapor entering or exiting the control volume due to evaporation or condensation. Darcy's Law is written with saturation as the dependent variable

$$\dot{m} = \frac{\rho A_w K K_r}{\mu} \frac{dP_c}{dS} \frac{\partial S}{\partial x} \tag{2}$$

Inertia terms are neglected through the use of this relationship. This assumption is justified because of the extremely low velocities encountered in porous wick materials, and has been utilized in previous works.[7,8] The relationship between the mass of liquid in the control volume and the saturation is

$$m = \rho \varepsilon A_w \Delta x S, \tag{3}$$

where ε is the wick porosity and $A_w \Delta x$ is the volume of the element. When Eq. (2) and Eq. (3) are substituted into Eq. (1), we obtain

$$\dot{m}_v = \rho A_w \left[\varepsilon \Delta x \frac{\partial S}{\partial t} x + \frac{K}{\mu} \left(K_r \frac{dP_c}{dS} \frac{\partial S}{\partial x} x - \frac{\Delta x}{2} - K_r \frac{dP_c}{dS} \frac{\partial S}{\partial x} x + \frac{\Delta x}{2} \right) \right] \tag{4}$$

Dividing by $\rho A_w \varepsilon \Delta x$ and taking the limit as Δx tends to zero, we obtain the equation for the transient saturation distribution

$$\frac{\partial S}{\partial t} = \frac{\partial}{\partial x} \left(f \frac{\partial S}{\partial x} \right) + J \tag{5}$$

Eq. (5) has the same form as the one-dimensional, nonhomogeneous heat equation. Here the moisture diffusivity is given by

$$f(S) = - \frac{K K_r}{\mu \varepsilon} \frac{dP_c}{dS} \tag{6}$$

The moisture diffusivity $f(S)$ is calculated from Eq. (6) based on the measured capillary flow properties.[9] A curve fit of the falling capillary pressure data shown in Fig. 2 gives dP_c/dS. The relative permeability is estimated from Fig. 3 as $K_r = \phi^2$.

It should be noted that the saturation has previously been defined as varying between zero and one. In the present solution, saturation is allowed to take on values greater than one to account for mass storage in the condenser region. When a porous structure is fully saturated ($S = 1$) and additional liquid is introduced to the exterior, the excess liquid cannot enter the pores. It, therefore, has no effect on the capillary flow properties of the structure. These remain at the (constant) fully saturated values. In the present case the properties are evaluated at $S = 1$ if S becomes greater than one. Flow in the resulting puddle of liquid outside the wick is ignored.

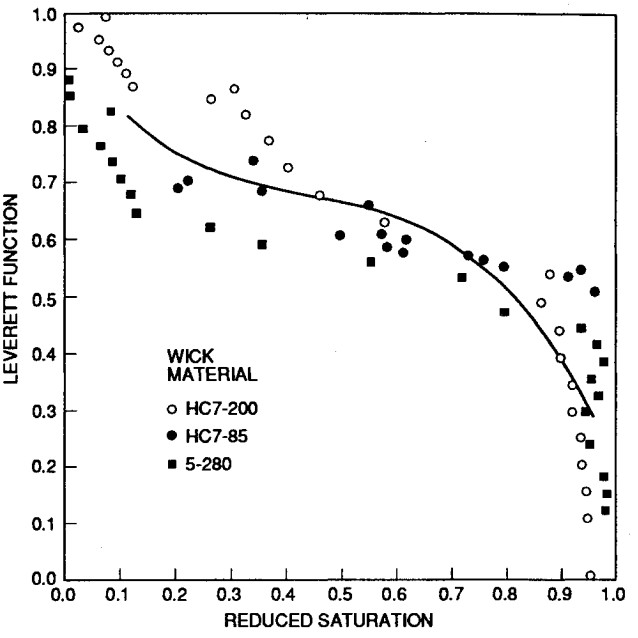

Fig. 2 Steady-state falling capillary pressure.

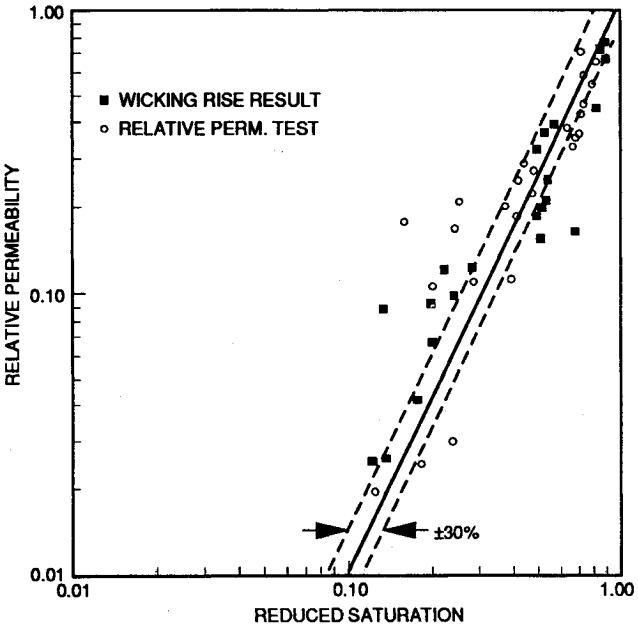

Fig. 3 Relative permeability data.

Source Term

The source term is the mass flux of vapor normalized by the initial mass of liquid per unit area of the void space. The total mass flow rate of vapor is given by

$$\dot{m}_{v,tot} = \frac{Q}{\lambda} \tag{7}$$

where Q is the heat transport rate. This is equal to the heat input if there is no storage of energy. The normalized mass flux of vapor is obtained by dividing the total amount by a

length. The source term is the evaporator region J_e is given by

$$J_e = -\frac{Q}{\rho\varepsilon A_w \lambda L_e} \tag{8}$$

Similarly for the condenser region

$$J_c = \frac{Q}{\rho\varepsilon A_w \lambda L_c} \tag{9}$$

Implicit in Eqs. (8) and (9) is the assumption that the vaporization and condensation are uniform over the evaporator and condenser, respectively.

Boundary and Initial Conditions

The boundary conditions state that no mass flow occurs through the two ends of the wick structure. This is the case in the actual heat pipe where the ends are sealed and recirculation of fluid occurs due to evaporation and condensation. From Eq. (2) this requires that $\partial S/\partial x = 0$ at $x = 0$ and $x = L_T$.

The initial condition for this problem is a uniform saturation equal to unity. This is the case in an actual, fully charged heat pipe assuming that the pipe has had sufficient time without heat loading and that the liquid wets the wick uniformly.

Numerical Solution

The complete problem specification is given as

$$\frac{\partial S}{\partial t} = \frac{\partial}{\partial x}\left\{f\frac{\partial S}{\partial x}\right\} + J,\ 0 \le x \le L_T\ S(x, 0) = 1$$

$$\frac{\partial S}{\partial x}(0, t) = 0, \frac{\partial S}{\partial x}(L_T, t) = 0$$

$$J = J_e;\ 0 \le x < L_e,\ t \ge 0$$

$$J = J_c;\ L_e < x \le L_T,\ t \ge 0$$

$$J = 0;\ x = L_e,\ t \ge 0 \tag{10}$$

The parabolic initial-boundary value problem Eq. (10) was solved numerically using the SPRINT package,[10] which is a general-purpose computer program for the numerical solution of mathematical models which involve mixed systems of time-dependent algebraic, ordinary, and partial differential equations. This package contains two spatial discretization options and four routines for performing the time integration. In the present work, the finite difference module SPDIFF was chosen for the spatial discretization and the time-stepping was performed using the SPGEAR module, which contains both the family of Adams methods up to order 12 and the family of Gear/backward difference formula (BDF) methods up to order 5. Details of these modules are given in Ref. 10. With these choices, SPRINT was run with various subdivisions of the spatial interval and various tolerances on the time integration. These results showed that the solution is relatively insensitive to the tolerance placed on the time integration. Based on the results, a time step of 1 s and 120 spatial intervals were deemed sufficient for the present problem.

Numerical Results

Results were obtained with values of the source term corresponding to heat inputs from 15 to 35 W. The input parameters used in the model are summarized in Table 1. The fluid properties were evaluated at a temperature of 40°C for all results. Transient saturation distributions are shown in Fig. 4.

The results from the numerical solution show a decreasing saturation in the evaporator region starting from $t = 0$. At power inputs of 30 W or greater, the saturation drops below the irreducible saturation of 15%. This corresponds to dryout of the wick in an actual heat pipe, since no flow can occur.

Beryllium-Wall Heat Pipe Tests

To verify the analytical model, direct measurements were obtained of the transient saturation distributions in an operating heat pipe. A beryllium wall heat pipe was designed and fabricated for this purpose. The heat pipe is shown in Fig. 5. Details of the saturation measurement using x-ray radiography are given in Ref. 9. Uncertainty of this measurement varies with the value of S, but is about 20% for $S > 0.1$.

Description of Apparatus

The heat pipe is constructed of copper, with two opposing beryllium walls through which the beam of x-rays may pass. The beryllium plates are sealed to the copper body with o-rings and held in place with top plates made of stainless steel. A copper tube is welded to one end of the body and attached to a valve used for evacuation and filling. At the other end is a brass feed through for the thermocouples used to measure interior temperatures during operation.

The wick material consists of five layers of square-mesh polyester fabric (22.8 threads per cm, No. 5-280) from Tetko, Inc. This material was cut to fit snugly in the cavity of the pipe against the bottom wall. The layers of mesh material were sewn together at numerous locations using polyester threads approximately 40 μm in diameter. In addition, it was necessary to use a wire mesh to provide uniform clamping pressure on the material so that it would remain planar and not develop excess space between layers. The wick is held tightly against the wall by a coarse stainless-steel mesh (3.1 wires per cm). This in turn is held down with special springs. The springs, made of copper-plated steel, are designed to minimize intrusion into the x-ray imaging area of the heat pipe.

A special heater was utilized for these heat pipe tests. This heater is a thin slab of carbon with copper contacts inserted through holes in the ends. A direct current is passed through the carbon, which is insulated from the beryllium wall by an extremely thin sheet of mica. The thin carbon heater allows imaging of the working fluid in the evaporator region of the heat pipe.

Internal temperature measurements are obtained from fine (0.003 in. diam.) copper/constantan thermocouples located inside the heat pipe. The wires have a fine coating of Isonel shellac insulation. There are 12 thermocouples, 10 located between the wall and the wick and two in the vapor space. The thermocouples are passed into the heat pipe through a 0.63 cm copper tube and ferrule fitting. Epoxy was used to seal the thermocouple wires into the tube. This arrangement had been devised as the most feasible method of providing a leak-proof seal with such fine gauge thermocouple wires.

Table 1 Input parameters for detailed liquid flow model

Constants	Dimensions	Fluid Properties
$K = 7.88 \times 10^{-10}$ m^2	$A_w = 2.85 \times 10^{-5}$ m^2	$\mu = 5.5 \times 10^{-4}$ kg/m·s
$\varepsilon = 0.7$	$L_t = 30$ cm	$\rho = 1530$ kg/m^3
	$L_e = 13$ cm	$\lambda = 1.5 \times 10^5$ J/kg
	$\Delta x = 0.0025$ m	$\sigma = 1.7 \times 10^{-2}$ N/m
	$\Delta t = 1$ s	

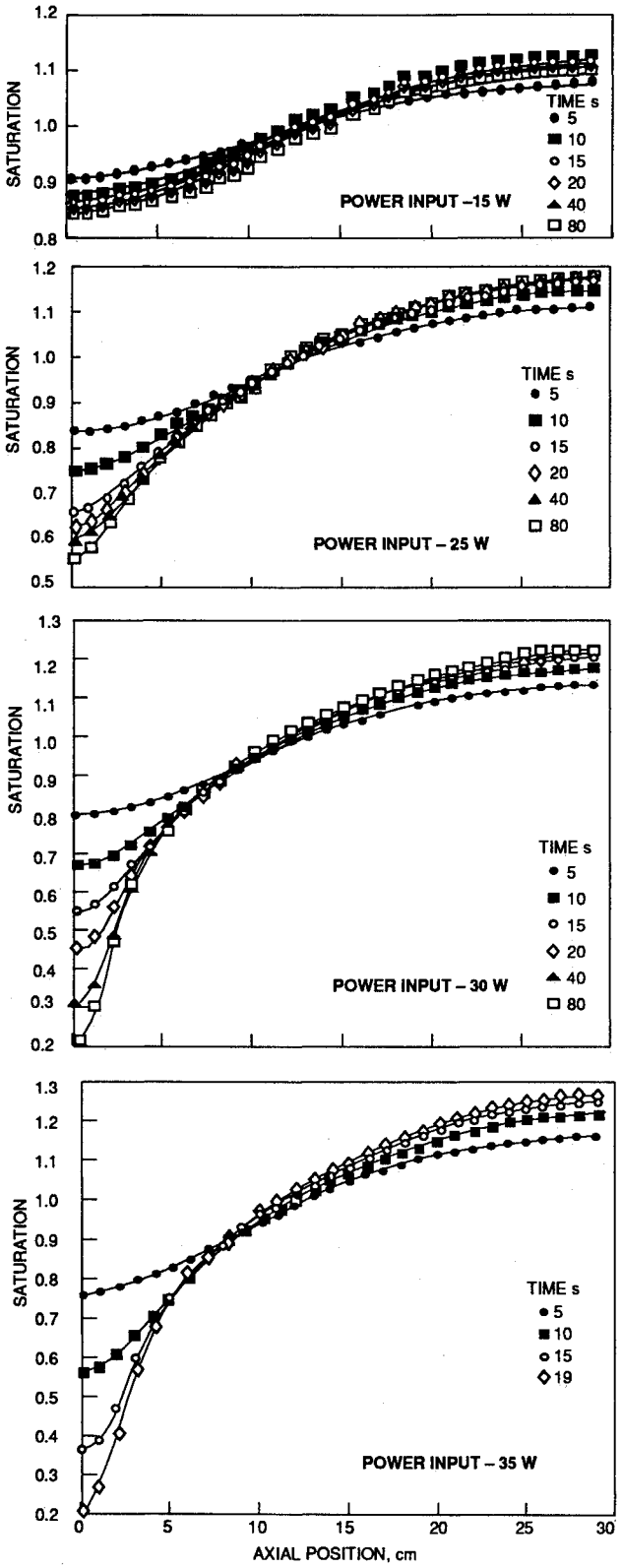

Fig. 4 Predicted transient saturation distributions.

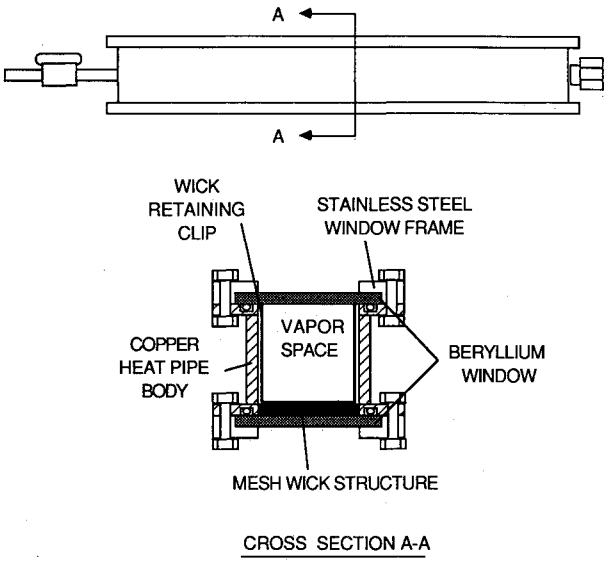

Fig. 5 Beryllium-walled heat pipe.

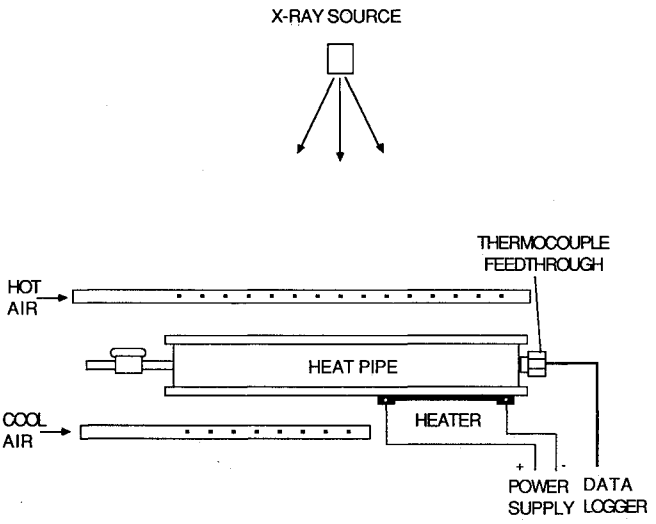

Fig. 6 Test set-up.

Heat Pipe Preparation

Prior to filling, the heat pipe was cleaned thoroughly in soapy water, followed by rinsing in methanol and then in Freon. It was closed, given a final rinsing with Freon, and then attached to the fill station. The heat pipe was evacuated to a pressure of approximately 100 μ of mercury and then filled with working fluid. The working fluid was then flushed into the evacuated liquid-nitrogen cold trap. The evacuation and fill procedure were repeated, so that the level of non-condensible gases in the heat pipe was reduced to a negligible level. The charge for the mesh wick of dimensions 29.2 cm $\times$ 1.9 cm $\times$ 1.5 mm and porosity of 69.9% is 6.15 ml of Freon-113.

The heat pipe was insulated with ceramic fiber insulation. Approximately 1.26 cm of the material covered all surfaces except the exposed beryllium windows. A thin layer (~0.63 cm.) of insulation was placed over the heater. This insulation was kept thin to reduce attenuation of x rays, already at its greatest in the heater region.

Heat Pipe Tests

The test setup consists of the heat pipe, the x-ray system, power supply, air flow system, and data logger. A schematic of the setup is shown in Fig. 6. The heat pipe is located in the x-ray chamber, with wires passed outside for the thermocouples and the heater. Two air lines are passed into the chamber, one hot and one room temperature. The hot air flowed onto the upper surface of the heat pipe to maintain it at a higher temperature than the Freon vapor. This reduces the condensation on the upper surface which would decrease the accuracy of the saturation measurement. The room temperature air directed onto the lower surface at the condenser region provides heat removal. Because the heat pipe can transport only of the order of 10 W, natural convection or low flow rate forced air is sufficient to remove the heat.

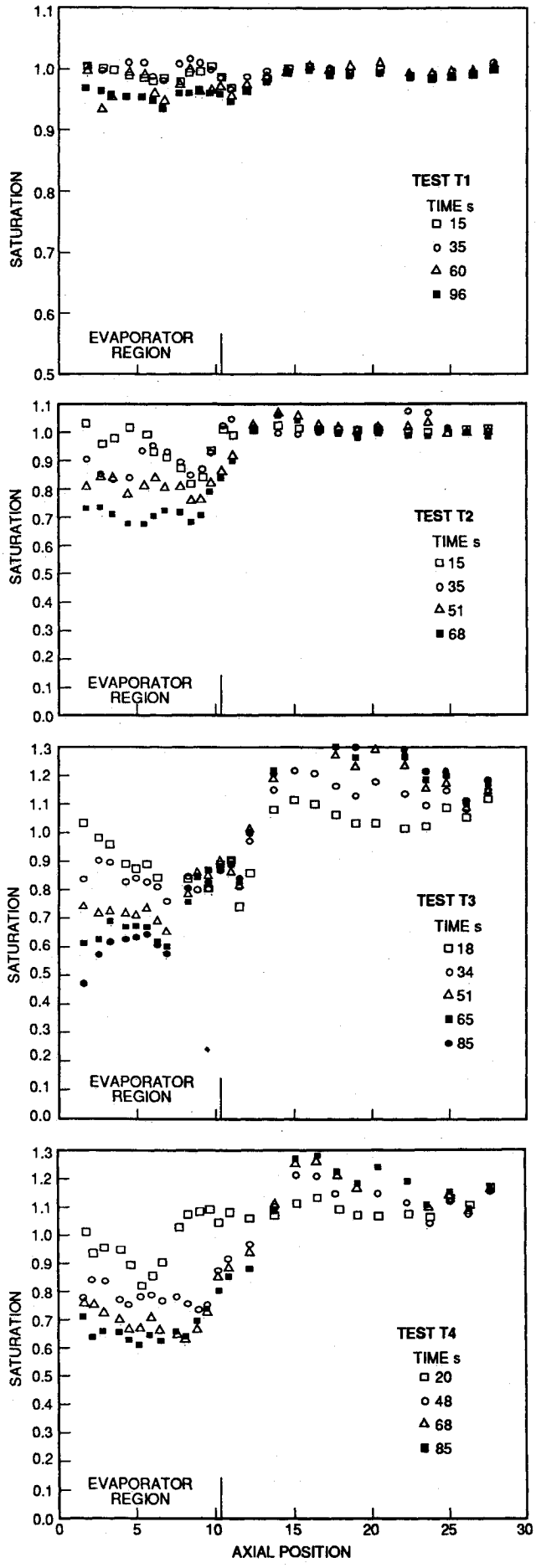

Fig. 7 Measured transient saturation distributions.

Both steady-state and transient experiments were performed. Experiments consisted of applying a fixed heat load to the evaporator of the pipe. At the same time, the power input and all temperatures were monitored using the data logger and x rays were taken at discrete time intervals to determine the saturation.

Transient Tests

Prior to each transient test, the heat pipe was heated to an initial temperature of 35–50°C using the hot air directed on the top surface. An initial radiograph was taken to verify a uniform saturation distribution prior to application of the heat load. The heat load was applied in one pulse. Radiographs were taken at intervals of roughly 15 s for the test duration, usually about 5 min. The exposure time of the tests was 2 s. For some tests, further radiographs were taken after heat input was removed to measure the increasing saturation in the evaporator zone. The results for the transient saturation distributions are shown in Fig. 7.

It was found that thermal energy storage could not be negated even though the pipe was initially hot. The pipe temperature was seen to increase moderately after the pulse of heat was applied. This rise in temperature was not uniform along the heat pipe. The estimated heat capacity of the heat pipe is about 425 J/°C. Therefore, even a small rise in temperature can account for a substantial fraction of the heat input. The heat storage, estimated from the time history of the average heat pipe temperature, was between 20 and 25 W. The estimated heat storage for each test was subtracted from the measured heat input. This correction provides a more accurate estimate of the heat-transport rate, but does not account for heat input from the hot air or heat losses from the pipe. The magnitudes of these are estimated to be lower than the thermal storage and the heat transport. The estimated heat-transport rate including the effect of storage is 20, 25, 30, and 35 W for tests T1, T2, T3, and T4, respectively.

The transient temperature profiles for the four tests are given in Fig. 8. Both internal and external temperatures are indicated on the graphs. Temperature difference ΔT_e between the evaporator wall/wick and the vapor is a measure of the actual heat transport by the heat pipe. The values for ΔT_e agree well with values predicted using a correlation of boiling heat transfer,[11] except for test T3. It is obvious that dryout of the wick occurred during this test from the steady increase in ΔT_e. From the transient saturation profiles for this test, it is seen that the largest reduction in saturation occurred for this test. The measured reduction in saturation is not as great as predicted by the model for a power input of 30 W. However, considering the larger uncertainty of the saturation measurement for smaller values of the saturation, the measured reduction is (within experimental uncertainty) close to the dryout condition (S = 0.15).

Steady-State Test

The steady-state test was an extension of a transient test. The heat input was continued for a period of about 30 min. A radiograph of the heat pipe was then taken to obtain a steady-state saturation distribution. The steady-state saturation distribution is shown in Fig. 9. The estimated heat input for this test was about 30 W. After this test it was found that about a third of the insulation on the heater had fallen off. This indicates that the heat losses were probably larger for this test and transient tests T1 and T4. The forced air on the condenser provides significant cooling of the heater in this case.

Comparison of Theoretical and Experimental Results

The results of the numerical solution compare fairly well with those of the heat pipe tests. The reason for the difference between the predicted and measured saturation distribution is the lack of detailed energy coupling in the liquid flow model.

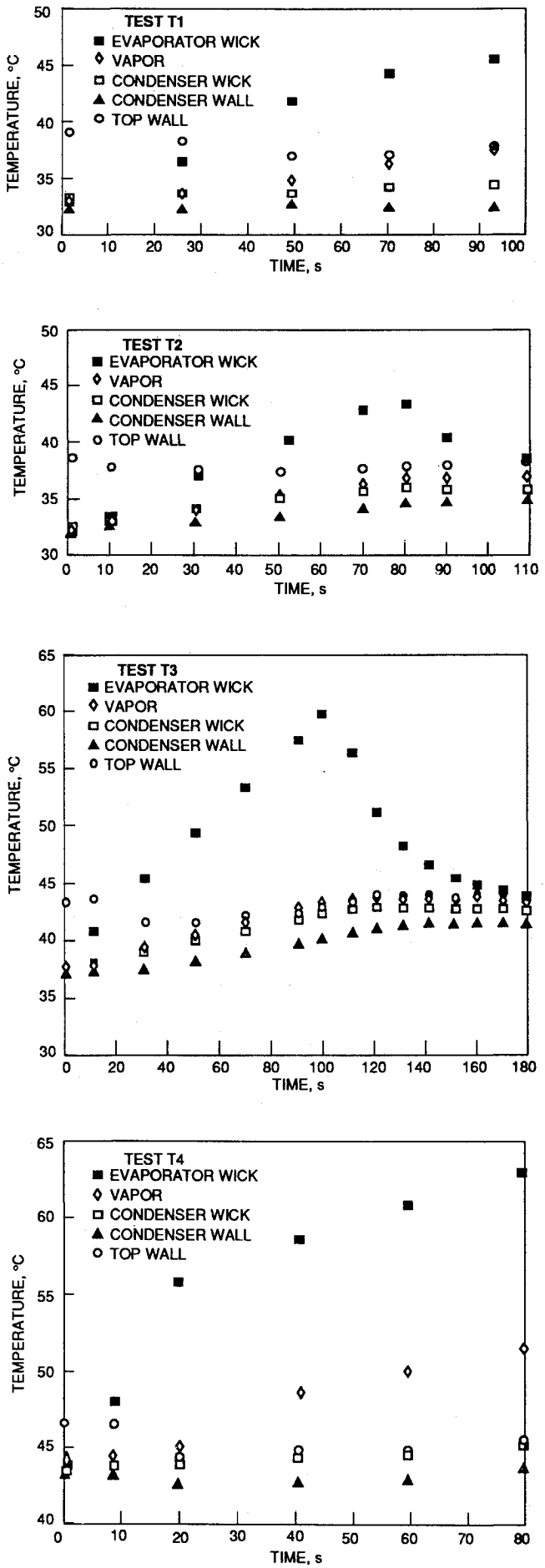

Fig. 8 Measured thermal response.

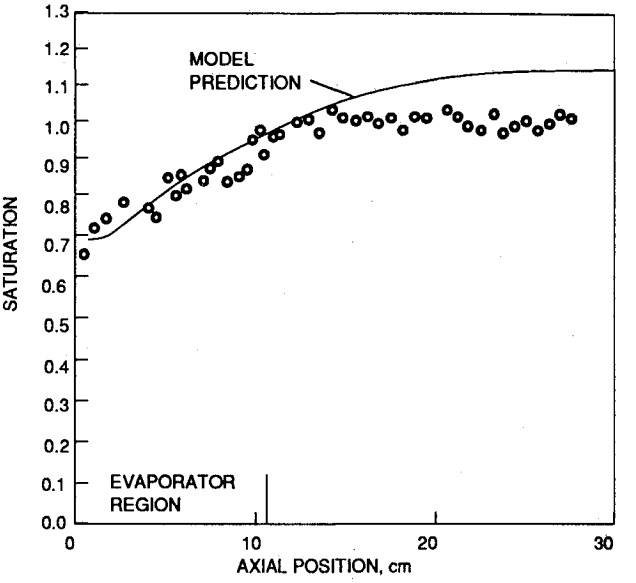

Fig. 9 Steady-state saturation.

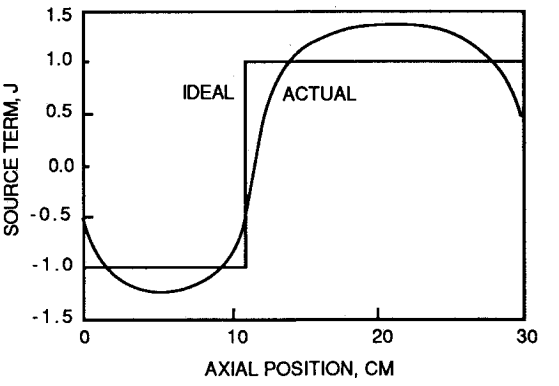

Fig. 10 Spatial dependence of source term.

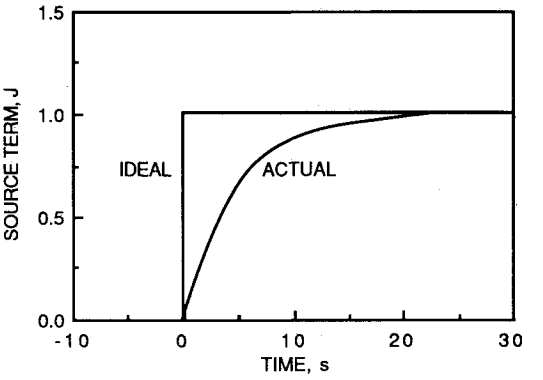

Fig. 11 Temporal dependence of source term.

The heat input to the heat pipe cannot be a step function of time and space as it is in the model.

The temperature of the wall measured near the heater (but in the condenser region of the wall) is greater than the average condenser wall temperature. This indicates that some heat is conducted along the wall to the condenser region. Because of this and the nonuniform thickness of the heater, the actual heat-input profile is not uniform. The qualitative behavior of the source term corresponding to the actual heat-input profile is compared in Fig. 10 to the idealized source term which is utilized in the solution of the liquid flow model.

The heater temperature increases dramatically during the first seconds of the pulse to overcome both the contact resistance and the thermal resistance of the insulator. The esti-

mated heat capacity of the heater is 14 J/°C. This means that the actual heat input to the heat pipe is less severe than the idealized source term utilized in the model, as shown in Fig. 11. The transient response in the experiment is controlled by the heat transfer instead of the liquid flow.

Because the actual heat input must vary continuously in space and time, there is a difference in shape between measured and predicted saturation distributions in the evaporator region. When overall energy storage is accounted for, the test results show similar reductions in saturation in the heated region to those predicted by the model.

Conclusions

A detailed study of transient liquid movement in heat pipe wicks has been completed. Saturation dependent properties were used in a transient liquid-flow model to predict liquid distributions in the heat pipe wick under pulsed heat-loading conditions. An experimental measurement of the liquid distributions in a heat pipe under pulsed loading conditions was performed to verify the model. The measured distributions compared favorably with those predicted using the model considering the nonideal nature of the experiment.

The results of the liquid flow model show that there is a rather steep drop in saturation in the evaporator region of the wick. This steep drop is also present in the experimental results. The nature of the measured distribution in the evaporator region is slightly different, these differences have been explained by the nonideal nature of the heat input in the experiment.

The detailed liquid-flow model presented here is a more powerful predictive tool for transient operation than was previously available. The results have pointed out that there are significant saturation reductions in the evaporator of a low-temperature heat pipe, even under conditions of steady-state operation. The transient operation of the heat pipe thus depends upon the previous heat loading history because this determines the distribution of liquid within the heat pipe. The distribution affects the performance capability.

The new liquid flow model will allow more accurate modeling of the energy flow and temperature distributions. Previous energy modeling for low-temperature heat pipes have been lacking in regard to adequate description of the heat transfer in the wick. One important step forward was the recognition that boiling plays a major role[11] in the evaporative heat transfer. The present model will allow another important advance in the modeling of heat transfer in the wick to be made, namely, the saturation dependence of the wick thermal properties:

1) Using the liquid flow model, the significant changes in thermal resistance of the wick in the condenser can be modeled. When excess liquid is present, the conduction across this layer increases the temperature drop across the wick.

2) Temperature increases in the evaporator region during dryout can be more accurately modeled if the extent of the dry region is known. Prescription of the boundary condition at the interface between wall and wick during dryout requires detailed knowledge of the local saturation distribution.

Acknowledgments

This work was sponsored by the Air Force Aero Propulsion Laboratory. The work was performed at the University of Kentucky, Lexington, Kentucky.

References

[1]Moss, R. A., and Kelly, A. J., "Neutron Radiographic Study of Limiting Planar Heat Pipe Performance," *International Journal of Heat and Mass Transfer*, Vol. 13, No. 3, 1970, pp. 491–502.

[2]Merrigan, M. A., Keddy, E. S., and Sena, J. T., "Transient Performance Investigation of a Space Power System Heat Pipe," AIAA Paper 86-1273, presented at the 4th ASME/AIAA Joint Thermophysics and Heat Transfer Conference, Boston, MA, June 1986.

[3]Shishido, I., Oishi, I., and Ohtani, S., "Capillary Limit in Heat Pipes," *Journal of Chemical Engineering of Japan*, Vol. 17, No. 2, 1984, pp. 179–186.

[4]Boyer, R. L., Morgan, F., and Muskat, M., "A New Method for Measurement of Oil Saturation in Cores," *Transactions of the American Institute of Mining and Metallurgical Engineers*, Vol. 170, 1947, pp. 15–33.

[5]Morgan, F., McDowell, J. M., and Doty, E. C., "Improvements in the X-Ray Saturation Technique of Studying Fluid Flow," *Transactions of the American Institute of Mining and Metallurgical Engineers*, Vol. 189, 1950, pp. 183–194.

[6]Laird, A. D. K., and Putnam, J. A., "Fluid Saturation in Porous Media by X-Ray Technique," *Transactions of the American Institute of Mining and Metallurgical Engineers*, Vol. 192, 1951, pp. 275–284.

[7]Beam, J. E., "Unsteady Heat Transfer in Heat Pipes," PhD Dissertation, University of Dayton School of Engineering, Dayton, OH, 1985.

[8]Colwell, G. T., and Chang, W. S., "Measurement of the Transient Behavior of a Capillary Structure Under Heavy Thermal Loading," *International Journal of Heat and Mass Transfer*, Vol. 27, No. 4, 1984, pp. 541–551.

[9]Ambrose, J. H., Chow, L. C., and Beam, J. E., "Capillary Flow Properties of Mesh Wicks," *Journal of Thermophysics and Heat Transfer*, Vol. 4, No. 3, 1990, pp. 318–324.

[10]Berzine, M., and Furzeland, R. M., "A User's Manual for Sprint-Parts 1 and 2," Department of Computer Studies, Leeds University, England, Reports 199 and 202, 1986.

[11]Ambrose, J. H., Chow, L. C., Ponnappan, R., Beam, J. E., and Mahefkay, E. T., "A Boiling Heat Transfer Correlation for Heat Pipes," *Society of Automotive Engineers Transactions*, Vol. 94, Sect. 5, 1985, pp. 161–167.